Journal of Applied Physics ARTICLE pubs.aip.org/aip/jap

Probabilistic modeling of energy transfer in disordered organic semiconductors

Cite as: J. Appl. Phys. **136**, 084501 (2024); doi: 10.1063/5.0218020
Submitted: 8 May 2024 · Accepted: 12 August 2024 ·
Published Online: 28 August 2024

Gustavo Targino Valente[1,a)] and Francisco Eduardo Gontijo Guimarães[2]

AFFILIATIONS

[1]Federal Institute of Education, Science and Technology of Brasília—Brasília Campus, Brasília, DF 70830-450, Brazil
[2]São Carlos Institute of Physics, University of São Paulo, PO BOX 369, São Carlos, SP 13560-970, Brazil

[a)]**Author to whom correspondence should be addressed:** gustavo.valente@ifb.edu.br

ABSTRACT

The non-radiative energy transfer process governs the transport of excitons in organic semiconductors, directly affecting the performance of organic optoelectronic devices. Successful models describe this transfer in terms of energy donor–acceptor pair sites, in contrast to experimental photophysical properties, which reflect the average behavior of the molecular ensemble. In this study, an energetic and spatial probability density function is proposed to determine the average non-radiative energy rate for homotransfer processes. This approach considers the energetic-spatial distribution typical of disordered semiconducting polymers. The average homotransfer rate is significantly dependent on the energy of the donor site, allowing the identification of the photophysical process most likely to occur. Values of the order of 10^{11} s^{-1} were predicted and are consistent with experimental results. This approach was used to evaluate how the energy transfer efficiency in heterostructures is affected by the energy and position of the energy donor site. The model presented in this study can be explored in other organic systems to investigate exciton transport mechanisms in new organic optoelectronic device architectures.

I. INTRODUCTION

The optoelectronic properties of organic semiconductors have paved the way for diverse technological applications, including organic photovoltaic cells (OPVs),[1–3] organic light-emitting diodes (OLEDs),[4,5] and organic field-effect transistors (OFETs).[6–9]

Many interesting topics related to charge and exciton transport in organic semiconductors have been discussed over the years.[10–18] A crucial aspect of organic device performance is the exciton diffusion,[11,19] which are driven by multiple energy homotransfer processes, i.e., non-radiative energy transfer between chemically identical molecules. Diffusion of excitons occurs from the highest to the lowest energy states of the density of states (DOS), producing a downward energetic relaxation.[20]

In OPVs, excitons must diffuse to the acceptor charge heterojunction to generate charge carriers via exciton dissociation.[14] However, the exciton diffusion length (3 and 17 nm)[19,21,22] is less than the active layer thickness (order of magnitude 10^2 nm) and its diffusion occurs in all directions in amorphous organic semiconductors. Consequently, only a fraction of the excitons reaches the interface and contribute to charge generation in devices with planar charge-accepting heterojunctions.

An approach to overcoming this problem is to direct the exciton motion between consecutive layers of different materials via energy heterotransfer processes,[23] a term used for non-radiative energy transfer between chemically different molecules. To support energy heterotransfer, each material has a lower energy state than the previous one.

The competition between energy heterotransfer and homotransfer must be taken into account in this situation. Experimental evidence indicates that downward energetic relaxation due to homotransfer occurs within 2 ps for polyfluorene films,[24] implying rates on the order of 10^{11} s^{-1} of the same magnitude for energy heterotransfer. Therefore, near heterojunctions, the energy transfer pathways are (1) homotransfer to one of the energy states in the DOS and (2) heterotransfer to an energy state at the interface.

Analysis of these energy transfer mechanisms must include the average photophysical behavior of the molecular assembly under study. Interestingly, the experimentally accessed energy transfer rates

reflect the average values of the studied set. For instance, more than one million chromophores—considering the average segment length of eight monomeric units and volume equal to 2×10^{-2} nm^3—are expected for ultrathin polymeric films (thickness lower than or equal to 10 nm) in a small region of 200 × 200 nm (the size of one pixel) normally accessed in laser scanning confocal microscopy experiments. This value must be even higher for spectroscopic techniques with spatial resolution of the order of 10^{-3}–10^{-6} m, as in femtosecond and steady-state spectroscopy, for example.

The influence of lower energy states on the energy homotransfer process was interpreted by[25] in a study with polydioctylfluorene (PFO) films,

$$k(E_i) \propto \int_{-\infty}^{E_i} k(E)\rho(E)dE, \tag{1}$$

where $k(E_i)$ is the energy transfer rate of the donor chromophore (or donor site) i characterized by the energy E_i, $\rho(E)$ is the DOS, and $k(E)$ corresponds to the transfer rate between two chromophores.

This equation can be understood as the average rate for lower energy states if $\rho(E)$ acts as a probability density function associated with the energy distribution of the electronic states in the material. A comprehensive description requires considering not only the energy dependence but also the incorporation of details of the spatial organization of chromophores.

In this study, the average energy homotransfer rate is determined for disordered semiconductor polymer films, considering the energetic disorder and spatial distribution of sites in three dimensions. Initially, we present the main theoretical concepts involved in the non-radiative energy transfer process and the premises of the proposed mathematical model in which the probability density function is presented. Then, we demonstrate how the mathematical model can be used to determine the probability of finding a site with a certain energy value.

Subsequently, the average homotransfer rate is obtained for a PFO film, a blue-light-emitting polymer widely studied in organic electronics and whose photophysical properties are well known.[26–31] The disordered PFO was adopted as a study model. At this stage, the transfer to higher and lower energy states and the effect of temperature on this process are discussed.

Finally, the average homotransfer rate is applied to investigate the energy heterotransfer in a donor–acceptor organic heterostructure. The effect of energy and distance from the donor site on heterotransfer efficiency are explored in this last section.

II. THEORETICAL BASIS AND METHODS

A. Non-radiative energy transfer processes

A fundamental characteristic to describe energy transfer processes in semiconductor polymers is the conformational disorder generated by the rupture of the conjugation of π electrons, resulting from chemical defects and twists along the polymer chain. Consequently, there is a statistical distribution of conjugate segments of different lengths, each presenting an excitation energy, promoting the energetic distribution described by the Gaussian disorder model. In this model, the polymeric semiconductor is represented by exciton-carrying elements named by sites, whose DOS is described by the Gaussian function,

$$G(E) = \frac{N}{\sigma\sqrt{2\pi}} e^{-\frac{(E-\mu)^2}{2\sigma^2}}, \tag{2}$$

where N is the site density, σ is the standard deviation, and E and μ correspond to the energy and the mean distribution value, respectively. The site is adopted here as a model to describe a chromophore, which is characterized by its energy gap.

The energy homotransfer rate from the donor site to the acceptor is described by the Miller–Abrahams equation adapted for non-radiative energy transfer,

$$k_{T,\text{homo}} = k_{\text{Förster}} e^{-\frac{E_a - E_d + |E_a - E_d|}{2k_B T}}, \tag{3}$$

with the Förster rate via dipole–dipole coupling $k_{\text{Förster}} = k_r (R_{0,\text{homo}}/r)^6$, where k_r is the radiative decay rate ($\sim 10^9$ s^{-1}),[32] $R_{0,\text{homo}}$ is the Förster radius for homotransfer (1–3 nm for conjugated polymer), and r is the distance between the energy donor and acceptor sites. In the exponential term, E_a and E_d are the energies of the acceptor and donor sites, respectively, k_B is the Boltzmann constant (eV K^{-1}), and T is the temperature (K). The exponential is defined by parts: (1) equal to the Boltzmann factor $e^{-\frac{E_a - E_d}{k_B T}}$ for $E_d < E_a$, (2) equal to 1 for $E_d \geq E_a$.

The heterotransfer efficiency Φ_{hetero} is determined by

$$\Phi_{\text{hetero}} = \frac{k_{T,\text{hetero}}}{k_{T,\text{hetero}} + k_{nr} + k_r + \langle k_{T,\text{homo}} \rangle}, \tag{4}$$

where $k_{T,\text{hetero}}$ is the energy heterotransfer rate, and $k_{nr} \sim 10^{12}$ s^{-1} and $k_r \sim 10^9$ s^{-1} are the non-radiative and radiative decay rates, respectively. According to the Förster model, $k_{T,\text{hetero}} = k_r(R_{0,\text{hetero}}/r)$,[6] where $R_{0,\text{hetero}}$ is the Förster radius for energy heterotransfer. The term $\langle k_{T,\text{homo}} \rangle$ is the average homotransfer rate that will be determined in the present study. The efficiency of any other photophysical process can be determined similarly to Eq. (4) by replacing the rate in the numerator with the desired property. For example, the homotransfer efficiency can be expressed by $\Phi_{\text{homo}} = \langle k_{T,\text{homo}} \rangle / (k_{T,\text{hetero}} + k_{nr} + k_r + \langle k_{T,\text{homo}} \rangle)$.

B. General model considerations

Let us consider an organic heterostructure with (1) an amorphous polymer film characterized by DOS, where homotransfer processes will operate, and (2) an organic molecular system with low conformational disorder, which promotes narrow DOS, approximated by a single energy-accepting electronic state in heterotransfer. The sites in the homotransfer and heterotransfer processes are called homotransfer sites and heterotransfer sites, respectively. The heterostructure consists of an ideal planar heterojunction, i.e., there is no interpenetration between these materials, as shown in Fig. 1(a).

In addition, the sites must be uniformly distributed throughout the volume of the polymeric film; there is no accumulation of material in any direction, consistent with spin-coating films. Consequently, energy and spatial distributions are independent. Therefore, the Spatial

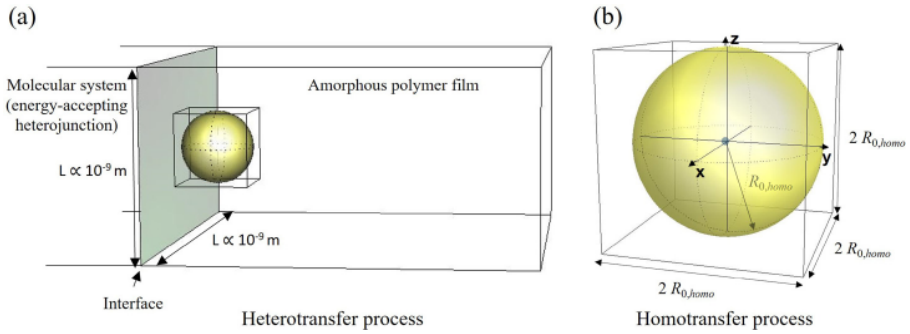

FIG. 1. Illustration of the system studied to describe hetero- and homotransfer processes. (a) Nanoscale dimension region composed of the amorphous polymer film on the right and the energy acceptor film on the left, forming an ideal interface indicated by the dark green region. This illustration also has a part of the film described by a cube containing a sphere, which is better detailed in the illustration alongside. (b) Region of the polymeric film delimited by a cube of length equal to $2R_{0,homo}$ containing a sphere in its center, delineated by the Förster radius $R_{0,homo}$, here called the energy transfer sphere. The energy donating site is in the center of the sphere.

Probability Density Function (SPDF) and the Energy Probability Density Function (EPDF) are also independent.

The geometric shape under analysis will be described by a cubic of nanometric dimensions with a donor site in the center so that the probability density functions (SPDF and EPDF) are equal in each portion of the volume. The energy donating site is understood as a site occupied by an exciton. Conveniently, a cube with a length equal to $2R_{0,homo}$ should be chosen to delineate a sphere, as indicated in Fig. 1(b), here called the energy transfer sphere. The sites contained in the energy transfer sphere are the potential energy acceptors in homotransfer.

From these assumptions, the SPDF for the energy transfer sphere is obtained from the transformation of the variables (x, y, z) to spherical coordinates (r, ϕ, θ) with $r \in (0, R_{0,homo}]$, $\phi \in [0, \pi]$, and $\theta \in [0, 2\pi]$. Then, SPDF is described by

$$H(r, \phi, \theta) = |J|h(x, y, z) = r^2 \operatorname{sen} \phi \frac{1}{(2R_{0,homo})^3}, \quad (5)$$

with $|J| = r^2 \operatorname{sen} \phi$ corresponding to the absolute value of the determinant of the Jacobian matrix and $h(x, y, z) = 1/(2R_{0,homo})^3$ corresponding to the product of the marginal distribution $1/(2R_{0,homo})$ of each independent variable x, y, and z.

EPDF is

$$g(E) = \frac{1}{\sigma\sqrt{2\pi}} e^{-\frac{1}{2}\left(\frac{E-\mu}{\sigma}\right)^2}, \quad (6)$$

which is related to the Gaussian DOS [Eq. (2)] by $G(E) = Ng(E)$. Note that EPDF is normalized; the probability (P) of finding a site with energy E for the entire sample space is $P[-\infty < E < \infty] = \int_{-\infty}^{\infty} g(E)dE = 1$.

Therefore, the joint probability density is expressed by

$$f(r, \phi, \theta, E) = H(r, \phi, \theta)g(E) = \frac{r^2 \operatorname{sen}\phi}{(2R_{0,homo})^3} \frac{e^{-\frac{1}{2}\left(\frac{E-\mu}{\sigma}\right)^2}}{\sigma\sqrt{2\pi}}. \quad (7)$$

The model considered only the temperature effects on energy transfer predicted by the Miller–Abrahams equation [Eq. (3)]. Any other temperature-induced alterations, such as expansion and thermal degradation, as well as breaks in the π-conjugation due to torsion in the polymer chain, were disregarded.

C. Methods

Using the $f(r, \phi, \theta, E)$, the average homotransfer rates were determined analytically with the support of Wolfram Mathematica software (version 11.2). To simulate the homotransfer results, the properties of the PFO given in Table I were used in the average homotransfer equations found in Sec. III. The average homotransfer values were used to obtain the efficiency of the photophysical processes using Eq. (4), which is detailed in Subsec. II A.

III. RESULTS AND DISCUSSION

A. Probability of finding a site

The integral over the entire sample space $\int_0^{R_{0,homo}} \int_0^{\pi} \int_0^{2\pi} H(r, \phi, \theta) dr d\phi d\theta$ indicates the probability of finding a site inside the energy transfer sphere. Its value corresponds to the ratio of the volume of the sphere to the volume of the cube, that is, $(4\pi R_{0,homo}^3/3)/(2R_{0,homo})^3$, which corresponds to $\pi/6 \cong 0.52$. It means that 52% of the sites uniformly distributed in

TABLE I. Properties of PFO film used to simulate the curves of average rates and heterotransfer efficiency. EPDF, energy probability density function.

Parameter		Value
Gaussian EPDF typical of PFO [$g(E)$]	μ	3.12 eV[a]
	σ	90 meV[a]
Radiative decay rate	k_r	10^9 s^{-1}[b]
Average homotransfer radius	$R_{0,homo}$	3 nm[c]

[a]Gaussian properties to reproduce the absorption spectrum of the PFO film.[33]
[b]Typical radiative decay rate for PFO films estimated using the decay time (~10^{-9} s).[26,34]
[c]Equivalent to the Förster radius.[24]

the $2R_{0,\text{homo}}$ edge cube will be involved by the energy transfer sphere.

$f(r,\phi,\theta,E)$ allows to know the probability of finding sites in a certain energy range present in a given volume within the energy transfer sphere. For instance, we will have a probability of approximately 36% of finding a site in the volume delimited by the energy transfer sphere for the energy range $\mu-\sigma<E<\mu+\sigma$ located around the center of DOS. Sites with energies within this range will be called dense states. On the other hand, the probability of finding sites with energies belonging to the DOS tail, with energies $E>\mu+2\sigma$ or $E<\mu-2\sigma$, is minimal and corresponds to approximately 1%. These sites with a probability lower than or equal to 1% will be called rarefied.

B. Average energy homotransfer rate

The average homotransfer rate $\langle k_{T,\text{homo}}\rangle$ in its most general form is calculated by

$$\langle k_{T,\text{homo}}\rangle=\frac{\int_0^{R_{0,\text{homo}}}\int_0^{\pi}\int_0^{2\pi}\int_{-\infty}^{\infty}k_{T,\text{homo}}(r,\phi,\theta,E)f(r,\phi,\theta,E)drd\phi d\theta dE}{\int_0^{R_{0,\text{homo}}}\int_0^{\pi}\int_0^{2\pi}\int_{-\infty}^{\infty}f(r,\phi,\theta,E)drd\phi d\theta dE}, \tag{8}$$

with $k_{T,\text{homo}}(r,\phi,\theta,E)$ corresponding to the homotransfer rate. The integral in the denominator corresponds to the normalization constant of $f(r,\phi,\theta,E)$ and is equal to $\pi/6$ considering the entire sample space in which the model was built, $r\in[0,R_{0,\text{homo}}]$, $\phi\in[0,\pi]$, $\theta\in[0,2\pi]$, and $E\in[-\infty,\infty]$. This integral will be replaced by this value for simplification purposes.

Although the probability density function depends on the variables (r,ϕ,θ), the $k_{T,\text{homo}}$ described by Eq. (3) is symmetric in ϕ and θ depending only on the distance r between sites. Figure 2(a) shows the behavior of the function $k_{T,\text{homo}}$ normalized by $(k_r)(R_{0,\text{homo}}/r)^6$.

The adopted approach will be to separately analyze the occurrence of energy transfer from a site with energy E_d to sites with lower $(E_d\geq E)$ and higher $(E_d<E)$ energies than E_d. Therefore, the average homotransfer rate for $E_d\geq E$ and $E_d<E$, respectively, can be written as

$$\langle k_{T,\text{homo}}\rangle_{E_d\geq E}=\frac{6}{\pi}\int_R^{R_{0,\text{homo}}}\int_0^{\pi}\int_0^{2\pi}\int_{-\infty}^{E_d}k_{T,\text{homo}}(r,\phi,\theta,E)\times f(r,\phi,\theta,E)drd\phi d\theta dE, \tag{9}$$

$$\langle k_{T,\text{homo}}\rangle_{E_d<E}=\frac{6}{\pi}\int_R^{R_{0,\text{homo}}}\int_0^{\pi}\int_0^{2\pi}\int_{E_d}^{\infty}k_{T,\text{homo}}(r,\phi,\theta,E)\times f(r,\phi,\theta,E)drd\phi d\theta dE, \tag{10}$$

considering that the lower limit of the integral in r must include $0<R<R_{0,\text{homo}}$ since $k_{T,\text{homo}}\to\infty$ when $r\to 0$. Furthermore, the selection of sites with energy below or above E_d is carried out by the limits of the integral of the energetic term. The limits of $E\in[-\infty,E_d]$ concern the case in which $E_d\geq E$; and $E\in[E_d,\infty]$ for the situation in which $E_d<E$. The validity domains of both equations are shown in Fig. 2 for a hypothetical energy E_d contained in the Gaussian DOS.

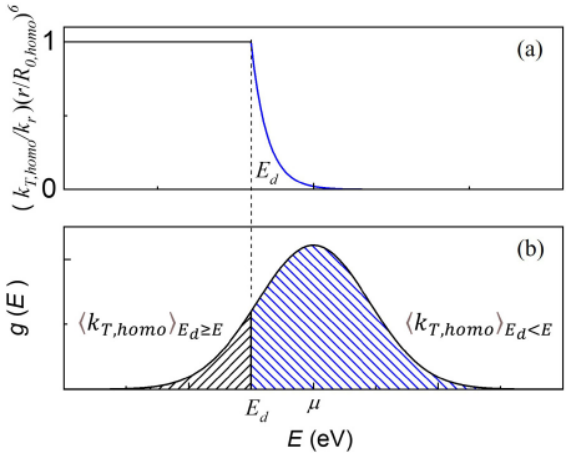

FIG. 2. (a) Behavior of $k_{T,\text{homo}}$ (normalized by the constants k_r and $R_{0,\text{homo}}$ and an arbitrary value of r) as a function of energy E with $E=E_d$ indicated by the vertical dashed line. The curve was simulated for thermal energy at room temperature, where k_BT is approximately equal to 26 meV. (b) It presents the EPDF that reflects the behavior of the Gaussian DOS with regions smaller (black dashed area) and larger (blue dashed area) than E_d in which Eqs. (9) and (10) are valid, respectively.

The result of the integral of the average homotransfer rate for the case in which $E_d\geq E$ is equal to

$$\langle k_{T,\text{homo}}\rangle_{E_d\geq E}=k_r\left[\left(\frac{R_{0,\text{homo}}}{R}\right)^3-1\right]\left(\frac{1+\text{erf}\left(\frac{E_d-\mu}{\sqrt{2}\sigma}\right)}{2}\right), \tag{11}$$

with $\left[\left(\frac{R_{0,\text{homo}}}{R}\right)^3-1\right]$ resulting from the integral of the spatial variables and $\left(\frac{1+\text{erf}\left(\frac{E_d-\mu}{\sqrt{2}\sigma}\right)}{2}\right)$ from the energetic variable, with $\text{erf}\left(\frac{E_d-\mu}{\sqrt{2}\sigma}\right)$ corresponding to the error function.

The dependence of $\langle k_{T,\text{homo}}\rangle_{E_d\geq E}$ as a function of energies E_d of the donor sites is shown in Fig. 3. EPDF is presented in the upper part of the figure. This curve was simulated considering the parameters shown in Table I. We assumed $R=0.34$ nm at the lower limit of the integral in r, which corresponds to a sphere with a volume equal to that predicted for a site (0.16 nm^3). This value will be used to simulate all subsequent curves. As expected, the rate is independent of thermal energy, as the transfer of excitons to lower energy states does not need to be thermally activated. Consequently, the exponential in Eq. (7) is a constant equal to 1, as indicated in Fig. 2(a). The average homotransfer rate for donor sites with energies equal to the average DOS, energy of 3.12 eV indicated by the black dashed line in the figure, presents the order of 10^{11} s^{-1}, which is about two orders of magnitude higher than the radiative decay rate (10^9 s^{-1}). Consequently, the exciton must

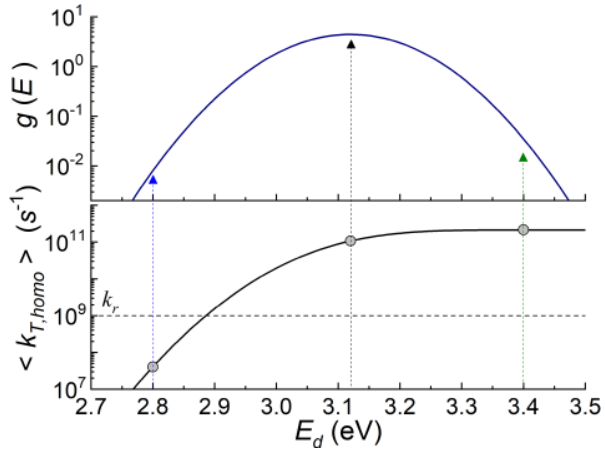

FIG. 3. Average homotransfer rate for sites with energies lower than E_d on a mono-log scale. The parameters used to simulate the curve are shown in Table I.

be transferred to some neighboring site contained in the energy transfer sphere, promoting exciton migration.

As the energy of the sites increases, the average homotransfer rate increases until it reaches a constant value of around $6.85 \times 10^{11}\ s^{-1}$, as indicated by the dashed green line in the figure.

In fact, these sites, belonging to the higher energy tail of DOS, have a higher number of sites available to accept the exciton. In other words, the density of sites with energy lower than E_d is high and, therefore, $\langle k_{T,\mathrm{homo}}\rangle_{E_d \geq E}$ is also high. On the other hand, the number of energy acceptor sites is rarefied when the donor site belongs to the lower energy tail of DOS (indicated by the blue dashed line) and, therefore, $\langle k_{T,\mathrm{homo}}\rangle_{E_d \geq E}$ assumes values lower than the radiative decay rate of $10^9\ s^{-1}$. Consequently, homotransfer will be unlikely and the radiative decay process will be dominant. That is, the exciton should practically not migrate during its lifetime and will occupy the same site until its radiative decay.

For the case in which $E_d < E$, the average homotransfer rate is expressed by

$$\langle k_{T,\mathrm{homo}}\rangle_{E_d<E} = k_r\left[\left(\frac{R_{0,\mathrm{homo}}}{R}\right)^3 - 1\right] e^{\left(\frac{E_d-\mu+\frac{\sigma^2}{2k_BT}}{k_BT}\right)} \times \mathrm{erfc}\left(\frac{E_d-\mu+\frac{\sigma^2}{k_BT}}{\sqrt{2}\sigma}\right)\frac{1}{2}, \quad (12)$$

in which erfc is the complementary error function, which is erfc $(w) = 1 - \mathrm{erf}(w)$, considering w equal to the argument of that function. The effect of thermal occupation given by k_BT for higher energy states is found in the complementary error function and the exponential that precedes it.

Figure 4(a) shows the behavior of $\langle k_{T,\mathrm{homo}}\rangle_{E_d<E}$ as a function of energy of the donor site at room temperature (~300 K), considering the parameters established in Table I. DOS is presented again at the top of this figure to indicate the location of energetic states in the distribution. The average homotransfer rate presents values higher than k_r for states with energies close to the center of DOS, as indicated by the black dotted line in the figure. It occurs due to the higher concentration of acceptor states within the energy transfer sphere can be thermally accessed. Consequently, the homotransfer

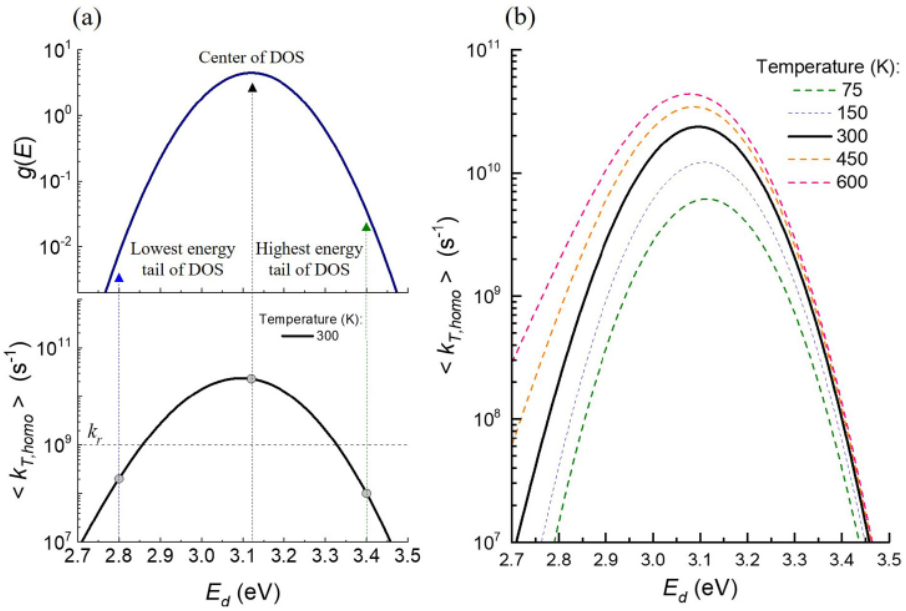

FIG. 4. (a) The energetic probability density $g(E)$ for the values in Table I is shown at the top, while the average homotransfer rate as a function of donor site energy E_d is shown at the bottom. Both figures are in a mono-log scale. (b) Effect of temperature on the average homotransfer rate.

process will predominate relative to radiative decay. On the other hand, the highest and lowest energy states (indicated by the dotted green and blue lines, respectively) present $\langle k_{T,\text{homo}}\rangle_{E_d<E}$ close to k_r; that is, the radiative decay process will compete with homotransfer.

The acceptor sites, that is, those with energies above E_d, are rarefied when a donor state belongs to the higher energy tail of DOS, and, therefore, the probability of finding an acceptor state within the transfer sphere will be small. For instance, the probability of finding a state with energy higher than 3.4 eV within the energy transfer sphere is 0.05% for $E_d = 3.4$ eV. In contrast, any state with energy higher than E_d that is within the transfer sphere is a candidate to receive the exciton if a donor state belonging to the lower energy tail of DOS. The probability of finding a state with an energy above this value is approximately 52% for an energy $E_d = 2.8$ eV. In other words, the number of candidates to accept energy will be abundant. However, only a portion of these states will actually accept energy since the transfer will only occur for those with energies close to that of the donor such that the thermal energy is sufficient to activate homotransfer. In this case, the number of acceptor states within the energy transfer sphere is controlled by temperature.

Consequently, the average homotransfer rate for these less energetic donor sites is affected by temperature, as shown in Fig. 4(b), which has $\langle k_{T,\text{homo}}\rangle_{E_d<E}$ for temperatures ranging from 75 to 600 K. Moreover, $\langle k_{T,\text{homo}}\rangle_{E_d<E}$ varies two orders of magnitude (10^8–10^{10} s^{-1}) for $E_d = 2.8$ eV, reaching values above k_r when the temperature increases from 75 to 600 K. In other words, homotransfer becomes more likely with the increase in the temperature, disregarding the effects of thermal degradation in the polymer material. A similar, but less pronounced, effect is observed for states in the center of DOS. However, thermal activation is ineffective for higher energy donor states, as energy acceptor candidates will continue to be rarefied even with an increase in the temperature.

C. Energy heterotransfer process

To study the efficiency of photophysical processes in the presence of homo- and heterotransfer, we assume that the heterotransfer sites located at the interface represent a single electronic state with lower energy than the donor, and, therefore, $k_{T,\text{hetero}} = k_r (R_{0,\text{hetero}}/r)$.[6] Let us also assume a fixed heterotransfer radius of $R_{0,\text{hetero}} = 12$ nm, independent of the energy of the donor site, to obtain the heterotransfer efficiency using Eq. (4). All calculations were done at a temperature of 300 K.

The vibrational relaxation process has rates of the order of 10^{12} s^{-1} and is generally dominant over all other processes; that is, it must occur before energy transfer and radiative decay. Therefore, analyzing the photophysical processes right after vibrational relaxation has occurred is convenient.

Figure 5 shows the ϕ_{hetero} behavior of a low-energy donor site (2.80 eV) as a function of its distance from the heterotransfer site at the interface. The illustration added to this figure depicts the situation in which the interface for heterotransfer is located on the left side in green color. The spheres in yellow represent the energy homotransfer sphere with the donor site in the center. The distances to the interface are as follows: I—3 nm, II—10 nm, and III—17 nm. This efficiency concerns the donor site and the closest heterotransfer site in the interface.

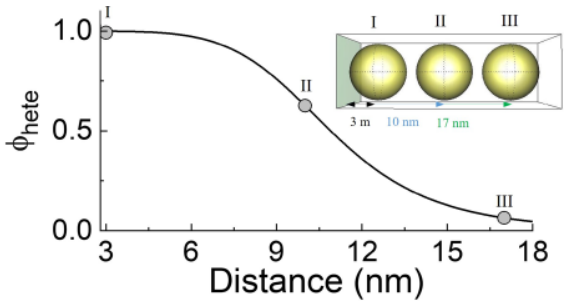

FIG. 5. Heterotransfer efficiency as a function of distance relative to the energy acceptor interface. The illustration included in the figure shows the energy acceptor interface (in green) together with the energy homotransfer spheres (in yellow) containing the polymeric site in its center. The distances relative to the interface are I—3 nm, II—10 nm, and III—17 nm. Simulated curve for $E_d = 2.8$ eV, $T = 300$ K, $R_{0,\text{hete}} = 12$ nm, and the PFO parameters in Table I.

The heterotransfer efficiency is influenced by the distance between the donor and the heterotransfer site. Maximum heterotransfer efficiency is observed for the energy acceptor interface when the site is at a distance equal to $R_{0,\text{homo}} = 3$ nm, a situation indicated by I. However, ϕ_{hetero} becomes smaller for higher distances so that this site demonstrates a 62% efficiency (situation II) for the limit of ultrathin films (distance equal to 10 nm), while the efficiency for higher distances presents lower values, still showing a value equal to 6% for situation III, for example.

The origin of the dependence of ϕ_{hetero} on distance is related to the competition between all photophysical processes, which depend on the donor site energy. Figure 6 shows the behavior of the efficiency of these processes (heterotransfer, homotransfer, and

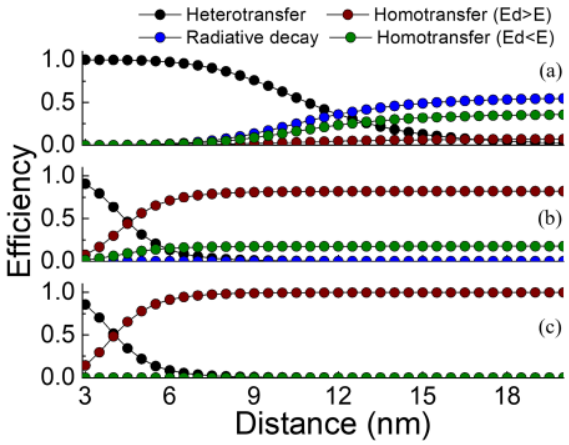

FIG. 6. Photophysical processes at room temperature for donor sites with energy equal to (a) $E_d = 2.80$ eV, (b) $E_d = 3.12$ eV, and (c) $E_d = 3.40$ eV.

radiative decay) as a function of distance between the donor and heterotransfer site. The energies of the donor sites are (a) 2.8, (b) 3.12, and (c) 3.40 eV, which correspond to states of the lowest, center, and highest energy tail of DOS, respectively.

The reduction in heterotransfer is followed by an increase in homotransfer efficiency as the distance between the donor and heterotransfer site increases. This is attributed to a reduction in $k_{T,\text{hetero}}$, making the heterotransfer pathway less relevant. Consequently, homotransfer efficiency increases to levels where there is no competition with heterotransfer. Note that $\langle k_{T,\text{homo}} \rangle$ is influenced only by the homotransfer site properties (energy and joint probability density) and is independent of the distance to the heterojunction, similarly for radiative decay.

Figure 6(a) shows that heterotransfer becomes dominant for distances less than 12 nm for a low-energy donor site. In contrast, the high average homotransfer rate $\left(\langle k_{T,\text{homo}} \rangle_{E_d \geq E} \cong 10^{11}\ \text{s}^{-1}\right)$ for a site belonging to the center of DOS implies competition with heterotransfer near the interface, a distance of around 4.5 nm from the interface, with efficiencies approximately equal to 45%, as shown in Fig. 6(b). The homotransfer process surpasses heterotransfer for distances higher than 4.5 nm and becomes dominant over all other processes.

Similar behavior is observed for a site with energy belonging to the highest energy tail of DOS, which presents efficiency of 51% and 48% for hetero- and homotransfer, respectively, at 4 nm from the interface [Fig. 6(c)]. These results indicate that the donor states with higher energies prefer to carry out the homotransfer process ($E_d > E$) for distances higher than 10 nm to a state of lower energy than to transfer to the heterotransfer site. Furthermore, homo- and heterotransfer processes are practically equivalent and compete with each other even close to the interface.

IV. CONCLUSION

In this study, the average rate of energy homotransfer was determined from the energy and spatial probability function for disordered polymeric films. This approach allowed to explore the mechanisms involved in the processes of homo- and heterotransfer of the energy.

The analytical expressions obtained for the average homotransfer rate indicate that this process is significantly affected by the energy donor. Average rates between 10^7 and $10^{11}\ \text{s}^{-1}$ were predicted, enabling the identification of the most likely photophysical pathway. Additionally, these findings have implications for the efficiency of photophysical processes in devices with planar energy-accepting heterojunctions. The heterotransfer efficiency depends on the donor site energy in conjunction with the donor–acceptor distance.

The results demonstrate that the heterotransfer efficiency is significantly enhanced when the low-energy homotransfer sites are situated at distances less than the exciton diffusion length (~10 nm) of the heterojunction. In this case, as the lower-energy sites are accessed at the end of exciton diffusion, the heterotransfer enables the perpetuation of exciton motion through additional layers. This theoretical prediction supports experimental approaches to direct exciton motion via energy transfer between planar heterojunctions.

The proposed model can be explored by adding temperature effects on the DOS of the homotransfer site. Furthermore, a DOS for the heterotransfer sites can be integrated into the model to derive an energetic and spatial probability density function for these sites. This will permit an investigation of other types of heterostructures, including bulk heterojunctions. The prediction of these processes can help in the planning of new, more efficient device architectures, contributing to the area of organic optoelectronics.

ACKNOWLEDGMENTS

The authors would like to thank the financial support provided by the São Paulo Research Foundation (FAPESP) through Process No. 2013/27047-7.

AUTHOR DECLARATIONS

Conflict of Interest

The authors have no conflicts to disclose.

Author Contributions

Gustavo Targino Valente: Conceptualization (equal); Formal analysis (equal); Funding acquisition (equal); Investigation (equal); Methodology (equal); Writing – original draft (equal); Writing – review & editing (equal). **Francisco Eduardo Gontijo Guimarães:** Formal analysis (equal); Funding acquisition (equal); Investigation (equal); Supervision (equal); Writing – original draft (equal); Writing – review & editing (equal).

DATA AVAILABILITY

The data that support the findings of this study are available within the article.

REFERENCES

[1]E. K. Solak and E. Irmak, "Advances in organic photovoltaic cells: A comprehensive review of materials, technologies, and performance," RSC Adv. **13**(18), 12244–12269 (2023).
[2]W. B. Tarique and A. Uddin, "A review of progress and challenges in the research developments on organic solar cells," Mater. Sci. Semicond. Process. **163**, 107541 (2023).
[3]H. Youn, H. J. Park, and L. J. Guo, "Organic photovoltaic cells: From performance improvement to manufacturing processes," Small **11**(19), 2228–2246 (2015).
[4]Y. Miao and M. Yin, "Recent progress on organic light-emitting diodes with phosphorescent ultrathin (<1 nm) light-emitting layers," iScience **25**(2), 103804 (2022).
[5]G. Hong, X. Gan, C. Leonhardt, Z. Zhang, J. Seibert, J. M. Busch, and S. Bräse, "A brief history of OLEDs—Emitter development and industry milestones," Adv. Mater. **33**(9), 2005630 (2021).
[6]X. Zhang, Z. Pu, X. Su, C. Li, H. Zheng, and D. Li, "Flexible organic field-effect transistors-based biosensors: Progress and perspectives," Anal. Bioanal. Chem. **415**(9), 1607–1625 (2023).
[7]L. Luo and Z. Liu, "Recent progress in organic field-effect transistor-based chem/bio-sensors," View **3**(1), 1–22 (2022).
[8]S. Yuvaraja, A. Nawaz, Q. Liu, D. Dubal, S. G. Surya, K. N. Salama, and P. Sonar, "Organic field-effect transistor-based flexible sensors," Chem. Soc. Rev. **49**(11), 3423–3460 (2020).

[9]I. Kymissis, *Organic Field Effect Transistors: Theory, Fabrication and Characterization*, 1st ed. (Springer US, Boston, MA, 2009), pp. 1–156.
[10]H. Bässler, "Charge transport in disordered organic photoconductors a Monte Carlo simulation study," Phys. Status Solidi B **175**(1), 15–56 (1993).
[11]O. P. Dimitriev, "Dynamics of excitons in conjugated molecules and organic semiconductor systems," Chem. Rev. **122**(9), 8487–8593 (2022).
[12]H. J. Eggimann, F. Le Roux, and L. M. Herz, "How β-phase content moderates chain conjugation and energy transfer in polyfluorene films," J. Phys. Chem. Lett. **10**(8), 1729–1736 (2019).
[13]S. D. Baranovskii, "Theoretical description of charge transport in disordered organic semiconductors," Phys. Status Solidi B **251**(3), 487–525 (2014).
[14]S. M. Menke and R. J. Holmes, "Exciton diffusion in organic photovoltaic cells," Energy Environ. Sci. **7**(2), 499–512 (2014).
[15]K. Müller, K. S. Schellhammer, N. Gräßler, B. Debnath, F. Liu, Y. Krupskaya, K. Leo, M. Knupfer, and F. Ortmann, "Directed exciton transport highways in organic semiconductors," Nat. Commun. **14**(1), 1–8 (2023).
[16]H. F. Haneef, A. M. Zeidell, and O. D. Jurchescu, "Charge carrier traps in organic semiconductors: A review on the underlying physics and impact on electronic devices," J. Mater. Chem. C **8**(3), 759–787 (2020).
[17]L. Pandey and M. Van der Auweraer, "Energy transfer dynamics in organic light emitting diode emission layers doped with triplet emitters," J. Appl. Phys. **110**(5), 053712 (2011).
[18]W. Zhou, C. Zimmermann, and C. Jungemann, "Master equation study of excitonic processes limiting the luminous efficacy in phosphorescent organic light-emitting diodes," J. Appl. Phys. **125**(16), 165501 (2019).
[19]Y. Tamai, H. Ohkita, H. Benten, and S. Ito, "Exciton diffusion in conjugated polymers: From fundamental understanding to improvement in photovoltaic conversion efficiency," J. Phys. Chem. Lett. **6**(17), 3417–3428 (2015).
[20]F. Laquai, Y. S. Park, J. J. Kim, and T. Basché, "Excitation energy transfer in organic materials: From fundamentals to optoelectronic devices," Macromol. Rapid Commun. **30**(14), 1203–1231 (2009).
[21]R. R. Lunt, N. C. Giebink, A. A. Belak, J. B. Benziger, and S. R. Forrest, "Exciton diffusion lengths of organic semiconductor thin films measured by spectrally resolved photoluminescence quenching," J. Appl. Phys. **105**(5), 053711 (2009).
[22]A. Bruno, L. X. Reynolds, C. Dyer-Smith, J. Nelson, and S. A. Haque, "Determining the exciton diffusion length in a polyfluorene from ultrafast fluorescence measurements of polymer/fullerene blend films," J. Phys. Chem. C **117**(39), 19832–19838 (2013).
[23]M. T. Sajjad, A. Ruseckas, and I. D. W. Samuel, "Enhancing exciton diffusion length provides new opportunities for organic photovoltaics," Matter **3**(2), 341–354 (2020).
[24]S. C. J. Meskers, J. Hübner, M. Oestreich, and H. Bässler, "Dispersive relaxation dynamics of photoexcitations in a polyfluorene film involving energy transfer: Experiment and Monte Carlo simulations," J. Phys. Chem. B **105**(38), 9139–9149 (2001).
[25]M. Ariu, M. Sims, M. D. Rahn, J. Hill, A. M. Fox, D. G. Lidzey, M. Oda, J. Cabanillas-Gonzalez, and D. D. C. Bradley, "Exciton migration in β-phase poly (9,9-dioctylfluorene)," Phys. Rev. B **67**(19), 1–11 (2003).
[26]A. Monkman, C. Rothe, S. King, and F. Dias, "Polyfluorene photophysics," in *Polyfluorenes*, edited by D. Neher and U. Scherf (Springer, Berlin, 2008), pp. 187–225.
[27]A. W. Grice, D. D. C. Bradley, M. T. Bernius, M. Inbasekaran, W. W. Wu, and E. P. Woo, "High brightness and efficiency blue light-emitting polymer diodes," Appl. Phys. Lett. **73**(5), 629–631 (1998).
[28]L.-L. Chua, J. Zaumseil, J.-F. Chang, E. C.-W. Ou, P. K.-H. Ho, H. Sirringhaus, and R. H. Friend, "General observation of n-type field-effect behaviour in organic semiconductors," Nature **434**(7030), 194–199 (2005).
[29]G. Heliotis, R. Xia, D. D. C. Bradley, G. A. Turnbull, I. D. W. Samuel, P. Andrew, and W. L. Barnes, "Blue, surface-emitting, distributed feedback polyfluorene lasers," Appl. Phys. Lett. **83**(11), 2118–2120 (2003).
[30]Q. Zhao, S. J. Liu, and W. Huang, "Polyfluorene-based blue-emitting materials," Macromol. Chem. Phys. **210**(19), 1580–1590 (2009).
[31]C. Yan, A. J. Cadby, A. J. Parnell, W. Tang, M. W. A. Skoda, D. Mohamad, S. P. King, L. X. Reynolds, S. A. Haque, T. Wang, S. R. Parnell, A. B. Holmes, R. A. L. Jones, and D. J. Jones, "Photophysics and morphology of a polyfluorene donor-acceptor triblock copolymer for solar cells," J. Polym. Sci., Part B: Polym. Phys. **51**(23), 1705–1718 (2013).
[32]T. Förster, "10th spiers memorial lecture. Transfer mechanisms of electronic excitation," Discuss. Faraday Soc. **27**(10), 7–17 (1959).
[33]G. T. Valente and F. E. G. Guimarães, "Simulation of the absorption spectrum of polydioctylfluorene" (unpublished).
[34]H. He, X. Liao, J. Cheng, Y. Li, J. Yu, and L. Li, "Investigation of energy transfer in star-shaped white polymer light-emitting devices via the time-resolved photoluminescence," Materials **11**(9), 1–13 (2018).